行政院國家科學委員會專題研究計畫成果報告

超音波諧波影像之研究

Study of Ultrasonic Harmonic Imaging

計畫編號：NSC 87-2218-E-002-052
執行期限：87 年 2 月 1 日至 87 年 7 月 31 日
主持人：李百祺　　台灣大學電機工程學系

一、中文摘要

超音波諧波影像，為利用人體組織之非線性反應所產生的第二諧波訊號，來提高影像品質的一個新影像技術。雖然此影像技術已在臨床上使用，但是受限於探頭的頻寬、系統的結構設計以及對於聲波在人體中之非線性傳遞的認知有限等諸多限制之下，諧波影像的品質仍有進一步提昇的空間。本計劃針對聲波在人體中的非線性傳輸建立了計算機模擬之模型。利用此模型，第二諧波訊號之聲場分佈，及新影像方法之效能，皆有深入的討論。

關鍵詞：超音波、非線性影像、諧波影像

Abstract

Harmonic imaging is used to image the second harmonic signal generated by the tissue nonlinearity and to improve image quality. Although its clinical importance has been verified, performance of second harmonic imaging is not yet optimal due to limited transducer bandwidth and system capabilities. In this project, we developed a computer simulation model for nonlinear propagation of sound waves. With this model, distribution of acoustic field and effects of new imaging techniques are explored.

Keywords: Ultrasound, Nonlinear Imaging, Harmonic Imaging

二、緣由與目的

A new application of harmonic imaging in diagnostic ultrasound is image formation based on finite amplitude distortion of the propagating beam [1,2]. Contrary to the conventional second harmonic imaging using contrast agents, no contrast agent is injected. Instead, harmonics are generated by the nonlinearity of tissue itself. It has been shown that sufficient harmonic signals can be generated at acoustic pressures within current safety limits [1]. In a homogeneous medium, sidelobes associated with the nonlinearly generated radiation pattern are much lower than those associated with the linearly generated radiation pattern. In an inhomogeneous medium, artifacts resulting from tissue inhomogeneities can also be significantly reduced. Therefore, finite amplitude distortion based imaging can be viewed as an alternative approach to improving spatial and contrast resolution in the presence of tissue inhomogeneities.

Although commercial products for second harmonic imaging have been available for clinical use, performance of such systems is not yet optimal. The primary limitations include transducer bandwidth, system programmability and the understanding of acoustic propagation in biological tissue. Therefore, it is the goal of this project to develop a computer simulation model for nonlinear propagation of sound waves under typical imaging conditions. In addition, new imaging techniques potential of further improving the imaging performance are explored with this simulation model.

三、方法

The simulation model accounts for pulse sources with arbitrary frequency response and approximates continuous beam formation by incremental field propagation. At each incremental step, linear propagation is calculated followed by nonlinear propagation. For linear propagation, the temporal waveform is first decomposed into discrete temporal frequency components. Then, the linear diffraction at each frequency is calculated using the angular spectrum method [3]. The nonlinear propagation over the same increment is obtained by using the frequency domain solution to Burgers' equation [4]. Due to the nonlinearity, harmonics and sub-harmonics generated by the nonlinear process alter the temporal frequency contents and affect subsequent wave propagation. In all simulations, propagation is assumed in water and no attenuation effect is included.

Let $u_i(x,y,z)$ represent the normal velocity field of an acoustic wave, where i is the temporal frequency index and (x,y,z) denotes the three dimensions in space. The velocity field can be decomposed into an angular spectrum of plane waves by taking two-dimensional Fourier transform with respect to spatial variables x and y. In other words, we have

$$U_i(f_x,f_y,z)=\int\int_{-\infty}^{\infty}u_i(x,y,z)e^{-j2\pi(xf_x+yf_y)}dxdy,$$

where $U_i(f_x,f_y,z)$ is the angular spectrum of $u_i(x,y,z)$, f_x and f_y are spatial frequencies associated with x and y, respectively. Since $u_i(x,y,z)$ obeys the Helmholtz equation (i.e., $(\nabla^2+k^2)u_i=0$, where k is the wave number), the angular spectrum at $z+\Delta z$ becomes

$$U_i(f_x,f_y,z+\Delta z)=U_i(f_x,f_y,z)H_i(f_x,f_y,\Delta z),$$

The function $H_i(f_x,f_y,\Delta z)$ is the propagation function defined as

$$H_i(f_x,f_y,\Delta z)=e^{jk\Delta z\sqrt{1-\lambda^2(f_x^2+f_y^2)}},$$

where λ is the wavelength at frequency i. The above equation indicates that the propagation function is essentially a spatial low pass filter. In the region where $f_x^2+f_y^2\le 1/\lambda^2$ (i.e., low spatial frequency region), the propagation function has a unity amplitude. Outside of this region (i.e., high spatial frequency region), the propagation function decays exponentially with increasing propagation distance. Waves of such spatial frequencies are also known as non-propagating waves due to the fact that they do not propagate effectively. Non-propagating waves can be ignored in simulations.

Let $u_i'(x,y,z+\Delta z)$ denote the temporary velocity field after linear propagation (i.e., the inverse two-dimensional Fourier transform of $U(f_x,f_y,z+\Delta z)$ with respect to f_x and f_y), the incremental nonlinear propagation is approximated by a plane wave process. Omitting variables x and y, the nonlinear propagation can be written as

$$u_n(z+\Delta z)=u_n'(z+\Delta z)+j\frac{\beta f\Delta z}{2c^2}$$
$$\left(\sum_{k=1}^{n-1}ku_k'(z+\Delta z)u_{n-k}'(z+\Delta z)\right.$$
$$\left.+\sum_{k=n}^{N}nu_k'(z+\Delta z)u_{k-n}'^{*}(z+\Delta z)\right),$$

where $u_n(z+\Delta z)$ is the result after both linear and nonlinear propagation, n is the temporal frequency index ($n=1,2,...N$), c is the sound velocity and f is the fundamental frequency of the waveform with a discrete frequency representation. In all simulations, β is set to 3.5 approximating the nonlinear property of water [5].

四、結果與討論

In all simulations in this paper, a one-dimensional, 96 channel linear array is assumed. The array has a 0.25mm pitch and the transmit focus is 50mm away from the transducer. Spectra of two representative waveforms are shown in figure 1. The solid line in figure 1 shows the spectrum of the

source plane velocity field. The signal has a Gaussian envelope with a 2MHz center frequency and a 50% fractional bandwidth. The source plane peak amplitude of the Gaussian waveform is equivalent to that of a continuous velocity field with a RMS acoustic intensity of 4W/cm^2. The dashed line shows the spectrum at the focal point. Second harmonic generation is evident as the harmonic amplitude is significantly increased. The second harmonic amplitude is about -23 dB relative to that of the fundamental frequency at the transmit focus. Note that such amplitudes may be too low compared to the system's dynamic range.

To improve the sensitivity, coded excitation is explored. Specifically, two chirp waveforms were simulated and compared to the Gaussian signal used in figure 1. The chirp waveforms used in this study have the following general form

$$S(t) = \exp(-\alpha(\pm t)^2)\cos(2\pi((f_0 - \frac{\Delta f}{2})t + \frac{\sim}{2}t^2)),$$

where $\exp(-\alpha(\pm t)^2)$ is a Gaussian function determining the envelope of $S(t)$, f_0 is the center frequency, Δf is the chirp bandwidth and $\sim$ determines the rate of change of the instantaneous frequency. Figure 2 shows a normal Gaussian waveform in the top panel and two chirp waveforms in the lower panels with normalized amplitudes. The normal Gaussian waveform is the same as the source plane signal used in figure 1. Parameters of the two chirp waveforms are chosen such that they have similar bandwidth and total pulse energy as the Gaussian waveform. The ratio of the peak amplitudes of the three waveforms is approximately 1:0.65:0.39 (from top to bottom) before being normalized for display.

Spectra of the three waveforms in the focal plane are shown in figure 3. The solid line represents the spectrum of the normal Gaussian waveform, the dashed line represents the spectrum of the short chirp waveform and the dot-dashed line represents the spectrum of the long chirp waveform. Clearly, the second harmonic amplitude decreases as the peak pressure decreases although the total pulse energy remains the same. The peak levels at the second harmonic frequency for the two chirp waveforms are about –3.7 dB and –8.2 dB relative to that of the normal Gaussian waveform. The reduction in second harmonic amplitude is consistent with the ratio of the on-axis, source plane peak amplitudes (i.e., 1:0.65:0.39). If the source plane peak amplitudes of the three waveforms are equal, figure 3 also implies that the SNR is improved by 3.7dB by using the short chirp waveform and by 8.2dB by using the long chirp waveform.

The SNR improvements using chirp waveforms are further illustrated in figure 4. The top panel depicts the axial amplitudes at the fundamental frequency and the bottom panel shows the axial amplitudes at the second harmonic frequency. In both panels, axial amplitudes of the normal Gaussian waveform, denoted by the solid lines, are compared to two chirp signals. The two chirp signals are identical to each other except for the peak amplitude. Compared to the normal Gaussian waveform, the first chirp waveform, denoted by the dot-dashed lines, has the same pulse energy but a lower peak amplitude. The second chirp signal, denoted by the dashed lines, has the same peak amplitude but higher pulse energy compared to the normal Gaussian waveform. Again, the dashed lines are very similar to the solid lines. The pulse energy in this case is about 3.7 dB higher than that of the normal Gaussian waveform. Hence, such waveforms can be used for finite amplitude distortion based imaging since they increase the SNR without exceeding the exposure limits.

Based on the above results, it is demonstrated that a simulation model has been successfully developed and the potential of coded excitation to further improve the performance of finite amplitude distortion based harmonic imaging has been verified. Although simulations were mainly performed for the finite amplitude distortion based harmonic imaging, the same techniques are

also applicable to microbubble based harmonic imaging.

Note that the simulations in this study only accounted for frequencies up to 6 MHz and effects of the higher frequencies were not included. Due to their relatively low amplitudes, however, it is expected that exclusion of higher harmonics does not have significant effects on the results.

五、計畫成果自評

Both linear and nonlinear propagation models were developed in this project. Moreover, simulations were performed using parameters typically seen in real imaging conditions. With this simulator, displaced and distributed aberrations can be included and effects of nonlinear propagation in the presence of tissue inhomogeneities can be investigated.

In addition to the project goals outlined in the proposal, potential improvement in imaging sensitivity of coded excitation was also explored using this simulator. The results have been submitted to Ultrasonic Imaging for consideration for publication.

六、參考文獻

[1] Christopher, T., Finite amplitude distortion-based inhomogeneous pulse echo ultrasonic imaging, *IEEE Trans. Ultrasonics, Ferroelec., Freq. Control UFFC-44,* 125-139 (1997).

[2] Christopher, T., Experimental investigation of finite amplitude distortion-based, second harmonic pulse echo ultrasonic imaging, *IEEE Trans. Ultrasonics, Ferroelec., Freq. Control UFFC-45,* 158-162 (1998).

[3] Goodman, J.W., *Introduction to Fourier Optics* (McGraw-Hill, New York, 1968).

[4] Haran, M.E., and Cook, B.D., Distortion of finite amplitude ultrasound in lossy media, *J. Acoust. Soc. Am. 73,* 774-779 (1983).

[5] Law, W.K., Frizzell, L.A., and Dunn, F., Determination of the nonlinearity parameter *B/A* of biological media, *Ultrasound Med. Biol. 11,* 307-318 (1985).

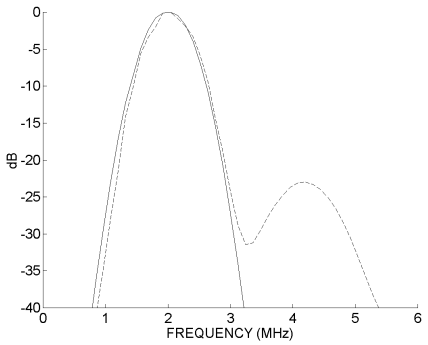

Fig. 1: Spectra at the source plane and at focus.

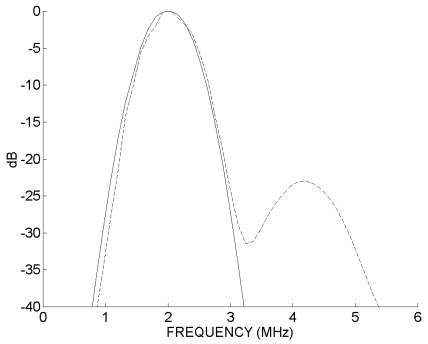

Fig. 2: Normal (top) and two chirp waveforms (middle and bottom).

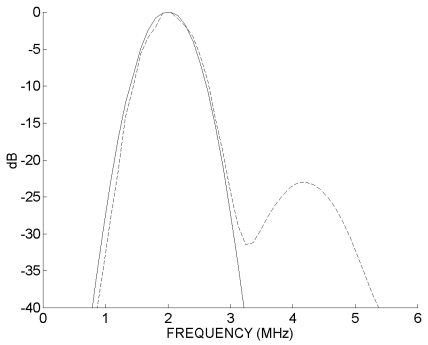

Fig. 3: Spectra at focus of the three waveforms in Fig. 2.

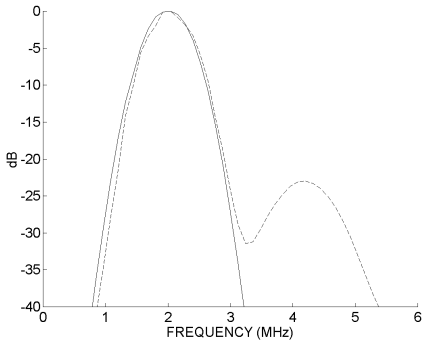

Fig. 4: On-axis amplitudes for fundamental frequency (top) and harmonic frequency (bottom).